ELSEVIER

The polarization of volcanic seismic signals: medium or source?

Margaret Hellweg *

Berkeley Seismological Laboratory, University of California at Berkeley, Berkeley, CA, USA

Abstract

With the proliferation of three-component seismometers on volcanoes, the temptation is great to use polarization analysis, as we do in earthquake seismology, to determine propagation direction and/or wavetype in order to locate and characterize the wave's source. In volcano seismology, there are two impediments to such a procedure: the complexity of the volcano's structure and the often long-lasting volcanic seismic signals. I develop a simple model of acoustic scattering and apply it to three simple, theoretical source signals, which represent the classes of signals encountered at volcanoes. When the medium is strongly scattering, the polarization at a receiver location for impulsive, sinusoidal or square-wave sources mimics the characteristics for volcanic shocks, tornillos with a single frequency and multichromatic tremor or tornillos. The polarization observed for the square-wave source resembles that observed for multichromatic tremor at Lascar Volcano, Chile, and multichromatic tornillos at Galeras Volcano, Colombia. At low frequencies, the particle motion is fairly linear and nearly constant, but cannot necessarily be used directly to indicate the direction to the source. At all frequencies, the particle motion exhibits some characteristics of Rayleigh waves, namely ellipticity of varying degrees and an 'RZ' product that oscillates with twice the frequency of the mode. If this model is correct, the lack of change of fundamental wavefield parameters, such as the polarization, for low frequencies during any given tornillo and from one tornillo to the next implies that the location of the source is stable to within a resolution of about 200 m.
© 2003 Elsevier B.V. All rights reserved.

Keywords: Galeras volcano; Lascar volcano; multichromatic tornillo; harmonic tremor; polarization analysis; scattering; scattered wavefield; covariance waveform analysis; waveform complexity

1. Introduction

Like weather forecasting at the beginning of the last century, monitoring efforts and activity forecasts for volcanoes have frequently been based on phenomenology, in effect matching patterns in the ongoing seismicity with patterns observed for past eruptions or explosions. Only recently, with improvements in the quality of seismic data due to increased bandwidth, high dynamic range, and perhaps most importantly, the availability of records from three-component seismometers, have we been able to begin to develop physical models for the sources of volcanic seismic signals. These models should help provide a physical basis for understanding the processes in a volcano, partic-

* Tel.: +1-510-642-8374; Fax: +1-510-643-5811.
  E-mail address: peggy@seismo.berkeley.edu (M. Hellweg).

ularly those relating to improved eruption monitoring.

Before we can proceed with modeling, however, we must face one of the fundamental problems in volcano seismology: Which signal characteristics are related to the source and which are influenced by the medium? It is clear that a volcanic edifice cannot be considered a simple medium with respect to wave propagation. The analysis of tremor or long-period volcanic events with extended codas as a means of studying their source is complicated by the passage of the seismic waves through this highly inhomogeneous edifice. We must carefully analyze these volcanic seismic signals to determine which of their characteristics describe parameters of the tremor source or the path. Only then can we develop source-related parameters into a realistic, physical model of the processes occurring within the volcano.

The spectra of volcanic tremor and events are often characterized by narrow-band peaks. When tremor is recorded using single-component, low-gain equipment, many questions about the tremor wavefield remain open. It is difficult to determine tremor parameters other than the frequency and amplitude from recordings of a vertical seismometer, or to distinguish between propagation effects and source characteristics. Without such discrimination, it is impossible to use tremor recordings to constrain models of physical or chemical processes in a volcano. Data from several three-component seismometers recorded with high dynamic range allow a more complete analysis of the tremor wavefield. As a result, tremor traits due to the source may be distinguished from those influenced by path and medium. The source-related parameters can then be used, along with source models, to determine the volcano's variables of state. Three time-varying characteristics of volcanic signals which can be measured using three-component seismograms are: the frequency, the total energy and the polarization.

Several phenomena affect the polarization of seismic waves. At their source, the polarization is, of course, determined by the source process – what we know as the source mechanism. At the recording site, the measured particle motion is influenced by the reflection at the free surface (Nuttli, 1961; Nuttli and Whitmore, 1961; Hellweg, 2000a; Neuberg and Pointer, 2000), the effects of topography (Neuberg and Pointer, 2000) and anisotropy along the path. Scattering in the medium is, however, also very important, as demonstrated by the coda we observe from events with impulsive sources, such as volcanic shocks or volcano-tectonic events (Aki and Chouet, 1975). How are long-lasting volcanic seismic signals, such as tornillos, hybrid events and volcanic tremor in its various forms (Schlindwein et al., 1995; Benoit and McNutt, 1997; Gómez and Torres, 1997; Hagerty et al., 1997; Lees et al., 1997; Hellweg, 1999a,b), affected by their passage through the medium? I develop here a simple, three-dimensional model of an acoustic medium with no intrinsic attenuation. Using it, I demonstrate the qualitative effects of scattering on impulsive wavelets, as well as on continuous sine and square waves. These are signal models for shocks, for tornillos with a single frequency and harmonic tremor or for tornillos and tremor with several frequencies, respectively.

2. Scattering in a heterogeneous acoustic medium

In the model, a three-dimensional grid of scatterers is embedded in an infinite, acoustic medium. Since the medium is infinite, there are no reflections from its boundaries. Because the medium is acoustic, it transmits only compressional waves. Although the volcanic medium is probably highly attenuating, this simple model does not include intrinsic attenuation. The scatterers are located at randomly selected nodes of the grid and their density can be varied. This model uses the Born approximation, which assumes that the scatterers are much smaller than the wavelength of the incident waves.

The velocity amplitude, $\dot{u}(r)$, of a spherically propagating, acoustic wave of frequency $\omega = 2\pi f$ from a point source in a homogeneous medium without scatterers in which the velocity of sound is c, is given by Ingard (1988):

$$\dot{u}(r) = \frac{U_0 a_0}{r} \frac{1 + \mathrm{i}/kr}{1 + \mathrm{i}/ka_0} \exp(\mathrm{i}kr - \mathrm{i}ka_0) \qquad (1)$$

In this equation, U_0 is the velocity amplitude as a function of time at the source–medium interface at radius a_0, while $k = \omega/c$ is the wave number. The wave propagating a distance r from an isotropically scattering monopole, s, at r_s takes on the same form:

$$\dot{u}_s(r) = \frac{\dot{u}(r_s)a_s}{r}\varepsilon_s\frac{1+i/kr}{1+i/ka_s}\exp(ikr-ika_s) \qquad (2)$$

with the exception that U_0 is replaced by $\dot{u}(r_s)$, the amplitude of the incident wave at the location of the scatterer, multiplied by the scatterer's efficiency, ε_s, and a_0 is replaced by the diameter of the scatterer a_s. For small values of ka_s, that is when the wavelength is much larger than the radius of the scatterer (Born approximation), the scatterer's efficiency is:

$$\varepsilon_s = \sqrt{\frac{\theta_s}{[(\theta+\theta_s)^2 + (\chi+\chi_s)^2]}} \qquad (3)$$

θ and θ_s are the normalized radiation resistance of the medium and the scatterers, while χ and χ_s are their respective reactances (Ingard, 1988). This number can never be greater than 1 and varies depending on the characteristics of the medium and scatterers (Ingard, 1988). In the model, each scatterer is randomly assigned a scattering efficiency, $0 < \varepsilon_s < 1$. This very simple model holds when the density of scatterers is low, so that the incident wave at any point in the model can be assumed not to have lost any energy to scattering. If the scatterers are more dense, the incident wave at the scatterer will have lost energy and have a lower amplitude than that given in Eq. 1. If the direct wave has traveled a distance r, the loss as compared to the wave amplitude with no scattering can be estimated as (Ingard, 1988):

$$C_{\text{scat}} = \exp\left(-\frac{r\langle\varepsilon^2\rangle\sigma_{\text{scat}}\rho_{\text{scat}}}{2}\right) \qquad (4)$$

where $\langle\varepsilon^2\rangle$ is the root mean square scattering efficiency, $\sigma_{\text{scat}} = 4\pi a_s^2$ is the scatterer cross-section and ρ_{scat}, the density of the scatterers, is taken to be the inverse of the cube of the mean inter-scatterer distance, d_{scat}.

The seismogram, $\dot{u}_0$, at the receiver location, r_0, is the sum of contributions from the source and from the single-scattering contribution of each point, s, of the scattering grid. For each node the incident amplitude is corrected for attenuation due to scattering using Eq. 4:

$$\dot{u}_0 = C_{\text{scat}}(r_0)\dot{u}(r_0) + \sum_{s=1}^{k}C_{\text{scat}}(r_s)\dot{u}_s(r_{s0}) \qquad (5)$$

where r_{s0} is the distance from the scatterer to the receiver and k is the number of scatterers.

If the source only radiates at a single frequency, i.e. a sine wave, it is easy to use Eq. 5 to calculate the outwardly propagating wave and the corresponding scattered waves in the time domain and superpose them at the location of the receiver to generate a synthetic seismogram for the configuration of scatters. If the source has a finite bandwidth, however, the problem becomes more difficult because of the frequency-dependent product $kr = \omega r/c$ in Eqs. 1 and 2. We therefore calculate the theoretical seismograms discussed in the following paragraphs in the frequency domain. First, the source seismogram is Fourier-transformed. For each scatterer, s, the spectrum is multiplied by the amplitude factors describing the geometric distance decay and the scattering losses and by the phase factors describing the phase shifts due to the distance traveled to the scatterer s. The spectrum is further multiplied by the scatterer's efficiency, and then the geometric distance decay factors and phase shifts to account for the separation between the scatterer and the receiver. The resulting spectrum for the contribution to the seismogram from the scatterer s is resolved into a radial component, parallel to the direction between the source and the receiver, and a transverse component perpendicular to it in a chosen plane. Since these calculations are made under the assumption of acoustic scattering, the radial and transverse components at the receiver location depend only on the direction between the scatterer and the receiver. The radial and transverse contributions for each scatterer in the scattering model are added to the radial and transverse receiver spectra of the direct wave before they are inverse Fourier-transformed to give the synthetic seismograms. The only disadvantage of this method is the acausality introduced by the manipulation of the spectra. It is due to the assumption made in spectral analysis that a signal repeats outside the

bounds of the interval analyzed. On inverse transformation, signal energy often 'leaks' from the tail of the signal to its beginning. In these synthetics, it is apparent as a low level of energy in the synthetic seismograms before the arrival of the direct wave.

For the examples shown below, the scatterers are randomly distributed throughout a volume $16 \times 16 \times 16$ km^3, with grid points every 200 m. The radius of the source and scatterers, a_0 and a_s are both taken to be 100 m, half the separation of the grid points, and the velocity of sound is $c = 1000$ m/s. The source–receiver distance is 4 km, unless otherwise noted. The source seismograms are normalized so that the amplitude of the unscattered signal would be 1 at the receiver, and that the product of the amplitude of the source and the source radius are approximately equal to the amplitude of the incident wave, excluding scattering attenuation, multiplied by the source–receiver distance, $U_0 a_0 \approx \dot{u}(r_0) r_0$

During the course of many trials, I varied three parameters, the density of the scatterers, ρ_{scat}, the efficiency of each scatterer, ε, and configuration of the scatterers. Tests for the density of the scatterers ranged from 0.0012 to 120 scatterers/km^3. Of course, the effect of scattering increases with increasing density. The figures which follow show examples for 0.12 scatterers/km^3, at which the effects of scattering finally become readily visible in the synthetic seismograms, and 12 scatterers/km^3, for which the synthetics for an impulsive source exhibit complexity similar to that observed in the seismograms of volcano-tectonic events. In these figures the efficiency of each scatterer is chosen randomly. While the specific shape of the synthetic changes when it is set to one for all scatterers, the qualitative results are affected very little. The same holds true for the configuration of the scatterers. The exact shapes of the synthetics change for different realizations of scatterers at a given density, but characteristics, such as the relative amplitudes of the radial and transverse components, remain the same.

What is the effect of scattering on different source waveforms? In the limiting case that there are no scatterers, the wavefield at the receiver is only radial, regardless of the duration and shape
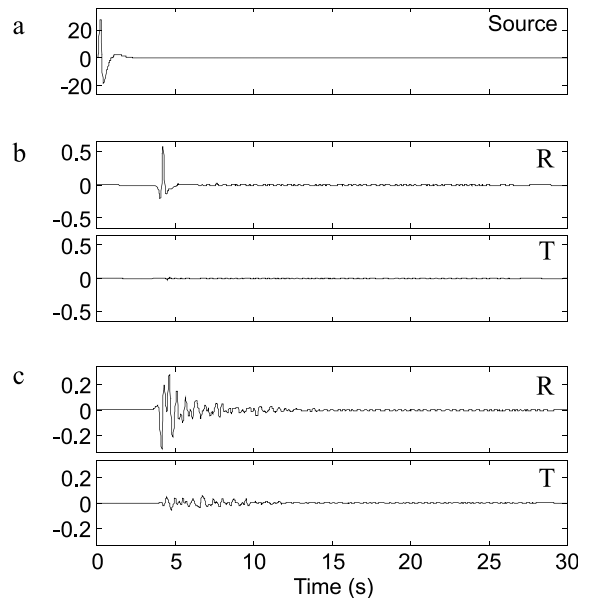

Fig. 1. Acoustic scattering for an impulsive source. (a) Source seismogram. (b) Radial (R) and transverse (T) synthetics for a weakly scattering medium, with $\rho_{scat} = 0.12$ scatterers/km^3, corresponding to a mean interscatterer distance of $d_{scat} = 2.0$ km. (c) Radial and transverse synthetics for a strongly scattering medium, with $\rho_{scat} = 12$ scatterers/km^3, corresponding to a mean interscatterer distance of $d_{scat} = 0.43$ km.

of the source function. With scatterers, the situation changes. For an impulsive source, like an earthquake or explosion (Fig. 1a), these effects are familiar to analysts as the coda. Far from being narrow-band, the spectrum of the impulsive source is broad-band, with contributions from many wave numbers, $k = \omega/c$. When the scattering density is small, $\rho_{scat} = 0.12$ scatterers/km^3, corresponding to a mean interscatterer distance of $d_{scat} = 2.0$ km, the coda is weak on the radial component and there is very little energy on the transverse component (Fig. 1b). The coda is effectively a transient which continues from the time of the arrival of the direct wave until waves reflected from the most distant scatterers have returned to the receiver location. After the incident wave has passed the most distant scatterers in this model, no more energy returns to the receiver, and the coda ends. Fig. 1c shows synthetics for a more densely scattering medium, $\rho_{scat} = 12$ scatterers/km^3, corresponding to a mean interscatterer dis-
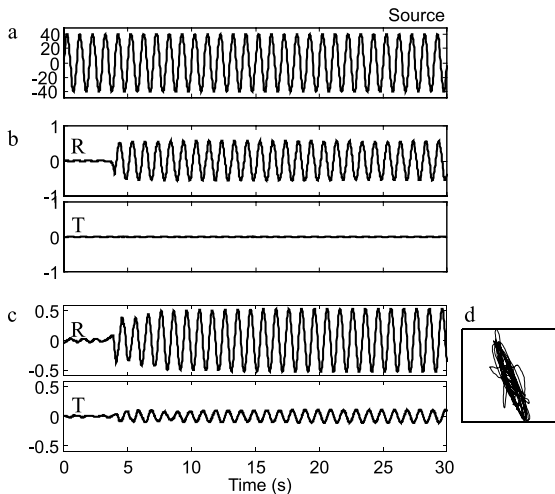
Fig. 2. Acoustic scattering for a monochromatic source. (a) Source seismogram. (b) Radial (R) and transverse (T) synthetics for a weakly scattering medium, with $\rho_{scat} = 0.12$ scatterers/km³, corresponding to a mean interscatterer distance of $d_{scat} = 2.0$ km. (c) Radial and transverse synthetics for a strongly scattering medium, with $\rho_{scat} = 12$ scatterers/km³, corresponding to a mean interscatterer distance of $d_{scat} = 0.43$ km. (d) Particle motion in the R–T plane during the transient in the strongly scattering medium.

tance of $d_{scat} = 0.43$ km. In this case, the simple, impulsive source function produces a seismogram similar to those measured for volcanic shocks, volcano-tectonic events and local earthquakes. The energy is partitioned between the radial and transverse components (Fig. 1c). The amplitude of the coda on the transverse component depends on the location and strength of the scatterers. When the density of scatterers is high, the maximum amplitude of the synthetic seismogram may be shifted from the onset to later in the seismogram, as it is in Fig. 1c.

Unlike shocks that are short and have an impulsive source, other volcanic seismic signals, such as simple tornillos and harmonic tremor, often continue for long intervals. A very simple example of such signals is tremor which has the appearance of a sine wave. These are narrow-band signals which begin at some time, $t = 0$ s, and then continue on indefinitely (Fig. 2a). If the density of scatterers is low, the wavefield at the receiver site is similar to that in a medium without scatterers (Fig. 2b). The seismograms are nearly radially po-

larized. When there are more scatterers, however, there is a transient after the initial onset (Fig. 2c). Like the coda for the impulsive source, this is the interval between the first arrival and the time in which the outwardly propagating wave reaches the limits of the scattering medium and the scattered waves from the most distant scatterers return to the receiver. During this interval, the amplitudes of both the radial and transverse components change as the effects of more scatterers join the signal. Unlike the case for the impulsive source, however, the sinusoidal source continues to radiate. The transient stops, at about 10 s in this model, when the first waves that have reached the limits of the scattering medium and been scattered have returned to the receiver. Then, there are no new contributions to the wavefield, which consists of the sum of the continuous source and all the scattered waves. The amplitudes of both components remain constant, as does their relative phase. In general, the ampli-
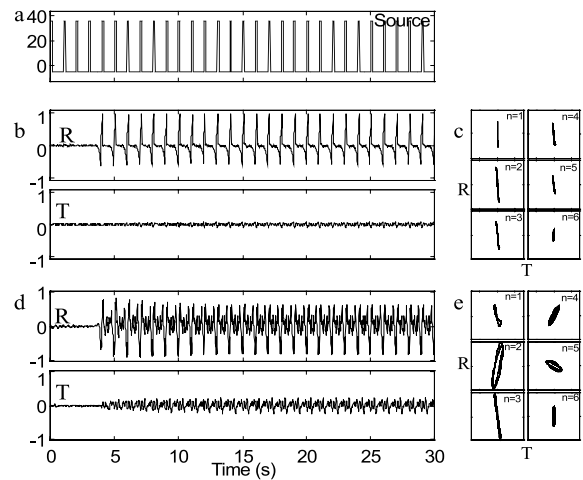

Fig. 3. Acoustic scattering for a multichromatic source. (a) Source seismogram. (b) Radial (R) and transverse (T) synthetics for a weakly scattering medium, with $\rho_{scat} = 0.12$ scatterers/km³, corresponding to a mean interscatterer distance of $d_{scat} = 2.0$ km. (c) Particle motion in the R–T plane at the frequencies of the first six spectral peaks for the weakly scattering medium. (d) Radial and transverse synthetics for a strongly scattering medium, with $\rho_{scat} = 12$ scatterers/km³, corresponding to a mean interscatterer distance of $d_{scat} = 0.43$ km. (e) Particle motion in the R–T plane at the frequencies of the first six spectral peaks for the strongly scattering medium.

tude and phase of the transverse component depend on the location and strength of the scatterers. If the transverse component is in phase with the radial component (Fig. 2d), the particle motion at the receiver site will be rotated from the radial and linearly polarized. The angle of rotation depends on the relative amplitudes of the two components. As the phase delay between the two components increases, the rectilinearity decreases. The particle motion is elliptical and the principal axis varies randomly, no longer necessarily pointing to the source.

The results for a square-wave source (Fig. 3a) provide insights into the effects of propagation on multichromatic wavefields, such as the multichromatic tremor at Lascar Volcano, Chile (Hellweg, 1999a, Hellweg, 2000a), and the multichromatic tornillos at Galeras Volcano, Colombia (Ortega, 2000). The square wave's spectrum is a sequence of narrow-band peaks, indicating that its wavefield is made up of waves with discrete wave numbers $k_n = \omega_n/c$. As in the case of the impulsive and sinusoidal sources, the transient is small when there are few scatterers and the waves arriving at the receiver are primarily radially polarized (Fig. 3b). Because there is little energy on the transverse component, each of the spectral lines is also radially polarized and highly rectilinear (Fig. 3c). When the number of scatterers increases (Fig. 3d), the transient after the onset lasts until the medium is saturated with outgoing and scattered radiation. The level of energy on the transverse component increases. At the same time, for a given scatterer the relative phase for the different peaks depends on the wave number, $k_n r$. Thus, when the spectra from many scatterers are superimposed at the receiver site, the polarization may be different for each spectral peak and is not necessarily related to the source–receiver direction (Fig. 3e), although the influence is smaller for longer wavelengths. The apparent amplitude of the seismic wave in the various bands is also affected by the scattering medium. If, by chance, the phase delays due to the scatterers result in cancellation or reinforcement, the amplitude may be nearly zero or much stronger than expected. An example can be seen by comparing the particle motion diagrams for $n = 3$ in Fig. 3c,e.
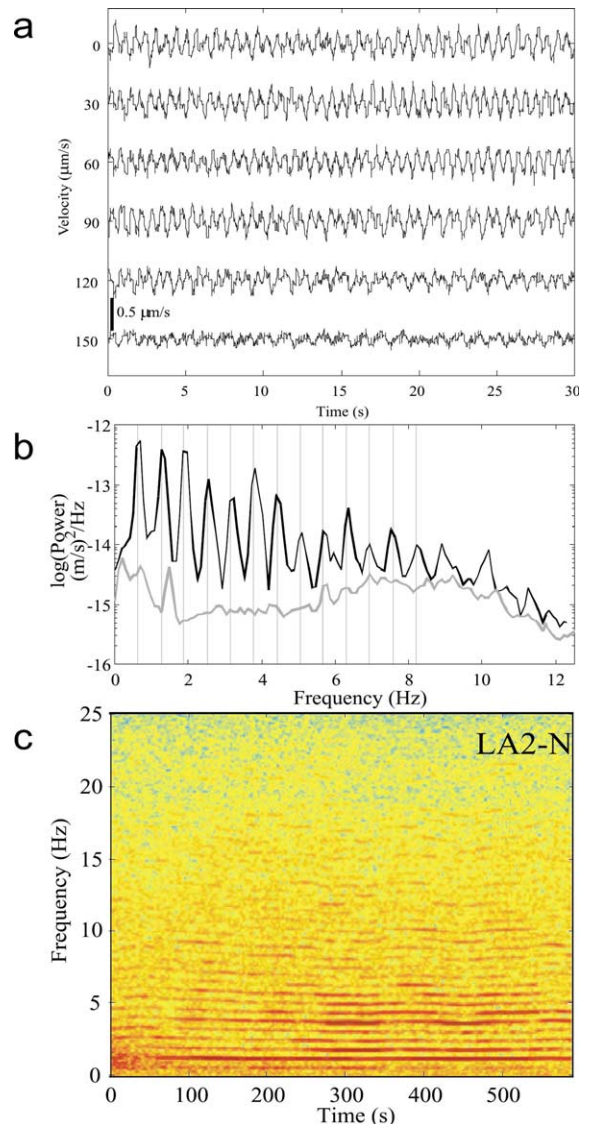

Fig. 4. Multichromatic tremor at Lascar Volcano, Chile, taken from the episode on 18 April 1994. (a) 3 min of tremor recorded on the *E* component at station LA2, about 4 km SSE of the active crater. Each trace shows 30 s of the 3 min window, with the starting time relative to the beginning given on the left axis. (b) Power spectrum of 10 min of multichromatic tremor calculated from the *N* component at the station LA2. The vertical lines are drawn at integer multiples of the frequency of the fundamental, 0.63 Hz. Note how well they match other peaks in the spectrum. (c) 10 min spectrogram of the *N* component at station LA2. Each spectral window is 10.24 s long and overlapped by 8.96 s.
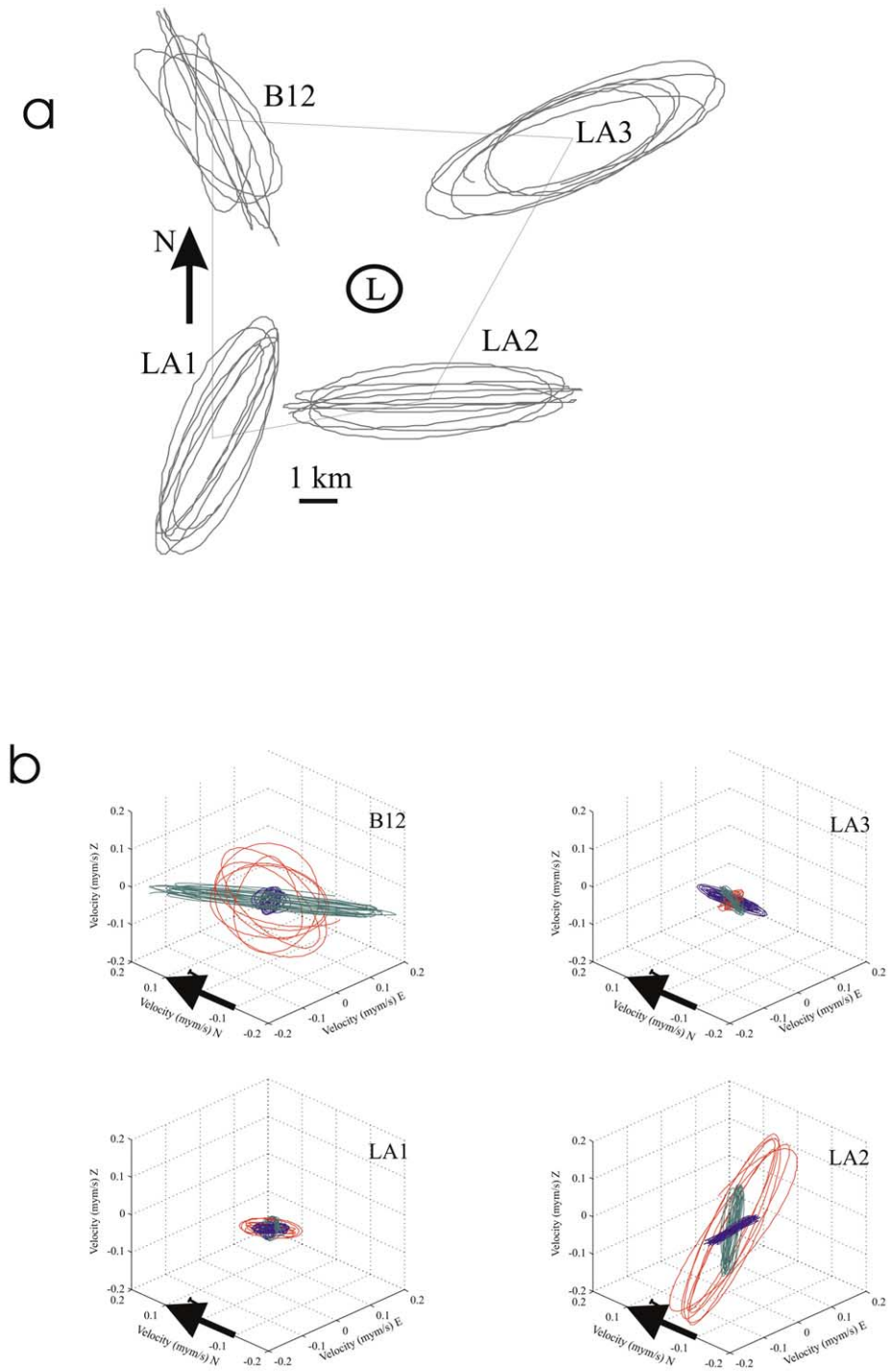
Fig. 5. Particle motion for 9.6 s of multichromatic tremor at Lascar Volcano, Chile. (a) Particle motion in the horizontal plane superimposed on a sketch of the station locations. The L is the approximate location of Lascar's active crater. (b) Three-dimensional representation of the particle motion for the same interval of data showing the polarization for the fundamental and the first two overtones.
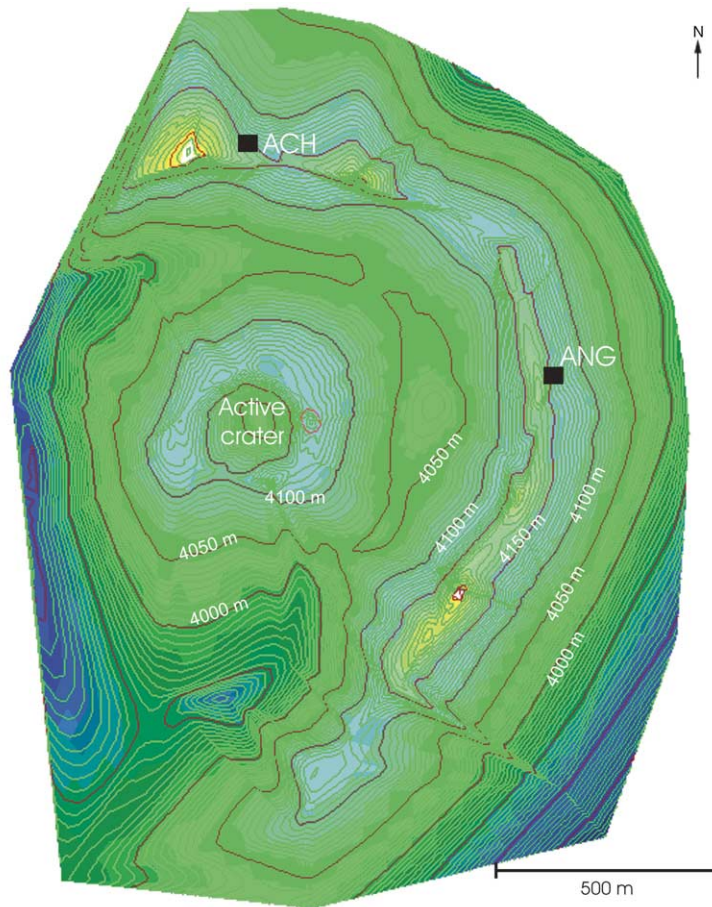
Fig. 6. Digital elevation model of the Galeras summit region. Squares show the locations of the two broad-band seismometer stations, ANG and ACH.

3. Example: multichromatic tremor at Lascar Volcano, Chile

Lascar, a stratovolcano more than 5000 m in altitude, is located on the puna, Chile's altiplano, at 23°22′S, 67°44′W. Gardeweg and Medina (1994) note that it is the most active volcano in northern Chile. Its activity is mainly fumarolic, although the continuous degassing is occasionally interrupted by large explosions from the various craters in the summit region. Since 1986, Lascar has undergone several cycles of lava dome growth and collapse. In April and early May of 1994, Asch et al. (1995, 1996) installed one broadband, three-component station and three short-period, three-component stations around Lascar Volcano.

The instruments at Lascar recorded a form of volcanic tremor characterized by harmonic spectra with a fundamental frequency near 0.6 Hz and many integer overtones with large amplitudes (Hellweg, 1999a,b, 2000a,b). In the time domain, this tremor is cyclic, with waveforms that change only slowly in shape and amplitude as a function of time (Fig. 4a). As this happens, the fundamental frequency changes, as does the frequency content (amplitudes of overtones). While the period of the cycle is the same at all stations, the contributions from the overtones are different on each component, resulting in different waveforms. Sim-
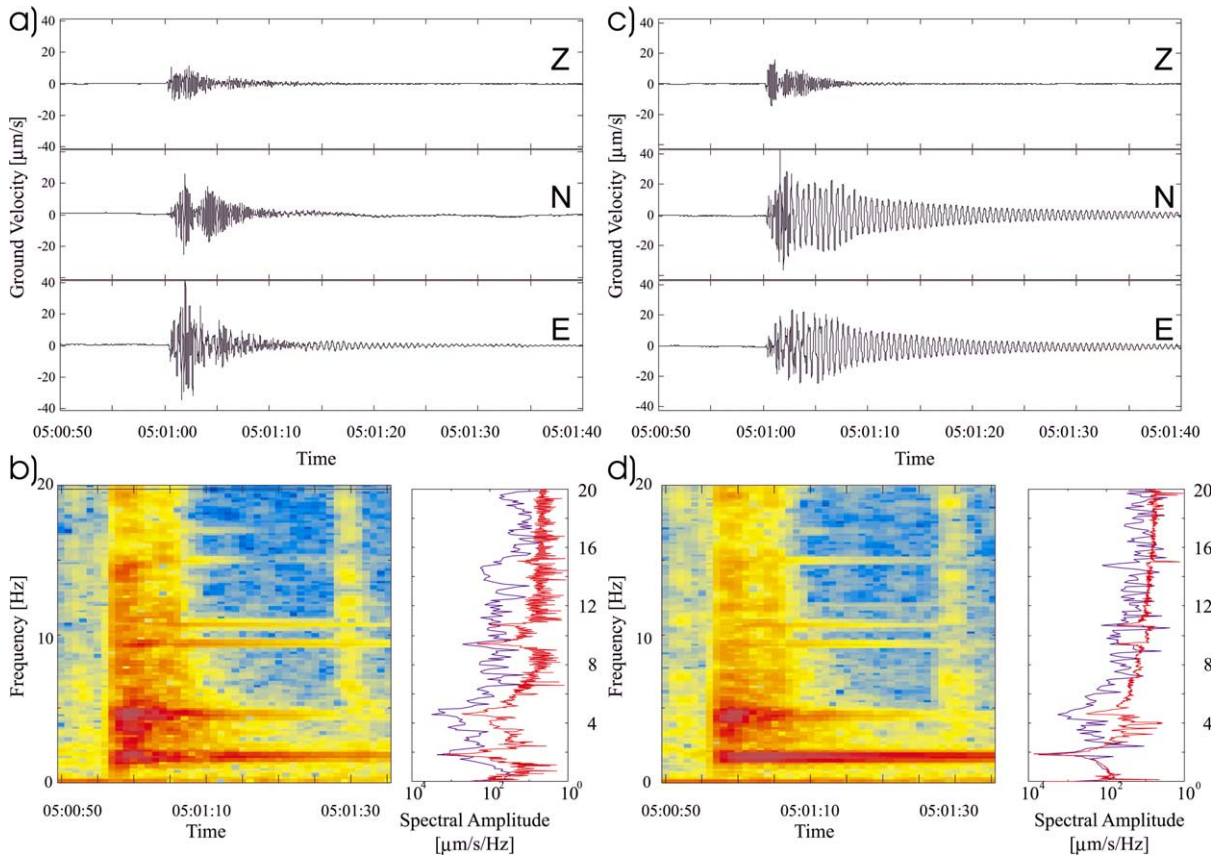
Fig. 7. (a) Bandpass-filtered seismograms (0.5–30 Hz) for the tornillo recorded at ANG at 05:00 UTC on 8 January 2000. (b) Spectrogram (5 s data spectral window with 2.5 s overlap) of the *E* component for the interval shown in panel a and amplitude spectra for the first 10 s of the tornillo (blue) and its coda (red). Note the spectral lines at around 2, 4, 9, 11 and 14 Hz. (c) Plot for the station ACH corresponding to panel a. (d) Spectrogram (5 s data spectral window with 2.5 s overlap) of the *N* component for the interval shown in panel c and amplitude spectra for first 10 s of the tornillo (blue) and its coda (red).

ilar tremor may have been observed at Galeras Volcano, Colombia, in 1989 (Gil-Cruz, 1999).

At Lascar Volcano, this continuous signal, like the square wave in Fig. 3a, is characterized by a spectrum with sharply defined peaks at a fundamental frequency, $f_1(t) = 0.63$ Hz, and numerous overtones at integer multiples, $f_n(t) = nf_1(t)$, where $n = 1, 2, 3,...$ (Fig. 4b). In the spectrogram of harmonic tremor (Fig. 4c) more than 20 overtones can be recognized. During the interval shown, the frequency of the fundamental varies only slightly, while the changes in the frequencies of the overtones are larger (Hellweg, 2000b).

4. The polarization of multichromatic tremor

For the fundamental frequency of harmonic tremor, Fig. 5a shows a 9.6 s interval of the particle motion in the horizontal plane for all four stations. The ellipses are superimposed on a diagram of the network, showing the locations of the stations relative to Lascar's active crater. Fig. 5b shows the three-dimensional particle motion for the fundamental (red) and the first two overtones. As predicted by the scattering model, the particle motion ellipses are not aligned nor are their relative amplitudes the same at all four stations. For

Table 1
Tornillo parameters

Date	Time	f [Hz]	ANG			ACH		
			α [°]	i [°]	rect	α [°]	i [°]	rect
010600	1225	1.90	254	85	0.91	221	90	1.00
		4.52	212	81	0.82	40	79	0.71
010700	0050	1.89	249	91	0.87	221	89	1.00
		4.16	217	77	0.77	38	69	0.70
		8.60	145	62	0.85	312	33	0.95
010800	0500	1.80	263	88	0.95	221	89	1.00
		4.61	224	88	0.77	342	72	0.48
		9.42	89	79	0.65	136	54	0.67
		10.71	19	36	0.61	49	72	0.73
		14.58	255	83	0.75	85	51	0.72
011000	0955	1.91	252	84	0.95	222	89	1.00
		3.75	278	71	0.71	223	88	0.55
		4.08	208	79	0.84	38	77	0.67
		9.96	75	55	0.18	23	87	0.47
		11.38	263	86	0.85	281	80	0.77
011300	0540	1.85	265	87	0.84	221	89	1.00
		3.71	277	72	0.80	213	87	0.48
		4.11	214	79	0.87	37	75	0.75
011400	1435	1.80	258	83	0.99	222	89	0.98
011700	0025	1.79	261	88	0.97	222	90	1.00
		9.07	223	58	0.66	145	69	0.80
		10.71	54	42	0.72	56	49	0.78
011700	2150	1.84	267	89	0.95	221	89	1.00
		3.74	257	75	0.81			0.18
		4.14	223	78	0.79	45	82	0.73
011800	1705	1.85	260	87	0.88	221	89	1.00
		3.72	269	73	0.77	222	74	0.63
011900	0635	1.82	263	83	0.96	221	90	0.97
		3.71	255	75	0.86			
		9.48	82	87	0.72			
012500	0310	1.75	256	84	0.97	223	89	1.00
		2.52	267	84	1.00	224	71	0.94
		10.18	49	10	0.76	22	75	0.91
		12.65	149	60	0.78	87	69	0.56
		18.05	315	15	0.79	260	83	0.77
020700	0500	1.91	252	89	0.96	223	90	1.00
		3.56	271	70	0.96	234	72	0.56
		9.94	281	23	0.43			
		11.34	272	69	0.92			
021000	1630	1.76	257	87	0.97	224	87	1.00
		3.71	258	77	0.90	238	84	0.86
		4.14	224	73	0.67	15	68	0.20
		7.36	251	74	0.77	183	70	0.94
		9.91	286	57	0.52	87	63	0.80
		13.15	91	68	0.35	46	82	0.87
		15.74	18	25	0.03	303	68	0.73
		19.28	103	51	0.77	316	81	0.83
021100	0330	1.75	260	89	0.99	223	89	0.99
		4.37	197	80	0.61	29	80	0.89
		11.84	92	52	0.52	18	78	0.88
		13.95	223	84	0.61			
		14.60	248	55	0.85			
021200	2150	1.75	260	89	0.99	223	89	0.99
		3.70	272	72	0.95	198	87	0.85
		10.19	254	19	0.68	192	82	0.97
		11.98	277	87	0.99	26	78	0.91
		14.28	253	11	0.70	98	43	0.68
		15.56	254	31	0.94	256	85	0.81
		19.46	55	78	0.95	86	84	0.96

example, while the fundamental has the largest amplitude at station LA2 (red), the amplitude of the first overtone (green) is largest at B12. The particle motion at the four stations cannot be jointly interpreted as a wavefield consisting solely of P-, S_V-, S_H- or Rayleigh-waves. This is typical for Lascar's harmonic tremor during other intervals as well (Hellweg, 1999b).

5. Example: multichromatic tornillos at Galeras Volcano, Colombia

Tornillos, observed at Galeras Volcano, Colombia, during the 1993 eruption cycles, are a particularly interesting specimen of volcanic seismic signal. On the one hand, like more typical seismic events with tectonic or explosion sources, their waveform has a clear onset and a definite duration. Unlike tremor they have a beginning and an end. They are much like tremor, however, in that they have an unusually high Q – that is, the coda is very long, and their spectra have only one or at most a few very sharp spectral peaks (Gómez and Torres, 1997). In the past decade, the tornillos at Galeras Volcano were observed to precede explosion eruptions (Torres et al., 1996; Narváez et al., 1997; Gómez and Torres, 1997; Ortega, 2000).

A suite of 42 tornillos occurred at Galeras Volcano between 8 December 1999 and 12 February 2000. All were recorded at the broad-band, three-component seismometer station ANG, which has been operating near Galeras' active cone continuously since July 1997 (Seidl et al., 2003), and those occurring after 5 January 2000 were also recorded at a second broad-band, three-component station installed to the north of the active crater (ACH, Fig. 6). These tornillos appear to be more complex than the tornillos previously recorded at ANG or those recorded with the short-period network of the Observatorio Volcanologico de Pasto. They are multichromatic, having narrow spectral peaks at up to nine, not necessarily harmonic frequencies. The tornillos' times and frequencies are listed in Table 1. Some of the peaks persist throughout the entire tornillo while others are only present during the first 10 s of the
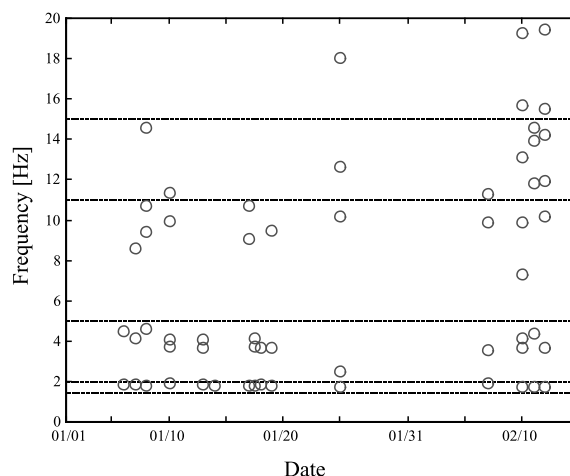

Fig. 8. Frequencies of the peaks present in the spectra of the tornillos recorded at the stations ANG and ACH between 5 January 2000 and 12 February 2000. The peaks are grouped by frequency: 1.5–2.0, 2.0–5.0, 5.0–11.0, 11.0–15.0 and 15.0–20.0 Hz.

tornillo. Here, we will analyze and discuss the polarization of the set of 15 tornillos recorded by both stations. The polarization and other signals characteristics observed for the 15 tornillos at the station ANG match those measured for the earlier tornillos of this suite, so the conclusions drawn from this set can be generalized to all 42 tornillos recorded during this episode.

The tornillo recorded on 8 January 2000 is one of the most complex tornillos, with peaks at five different frequencies (Fig. 7). In the recordings at both stations, energy is present in all five frequencies at the tornillo's beginning. It dies out rapidly, however, in the 4–5 Hz and 14–15 Hz bands, but continues in the 1.5–2, 9–10 and 10–11 Hz bands well into the coda. This can be seen in Fig. 7b,d, where separate amplitude spectra of the first 10 s of the tornillo and its coda are plotted beside the spectrograms.

In Fig. 8, we show the frequencies at which peaks occurred in each of the 15 tornillos recorded at both stations. It is apparent that all the tornillos have energy between 1.7 and 1.9 Hz, while many of them have peaks between 2 and 5 Hz. Just as the points for this peak represent a broader range of frequencies, each tornillo's peak in this range is much broader than for
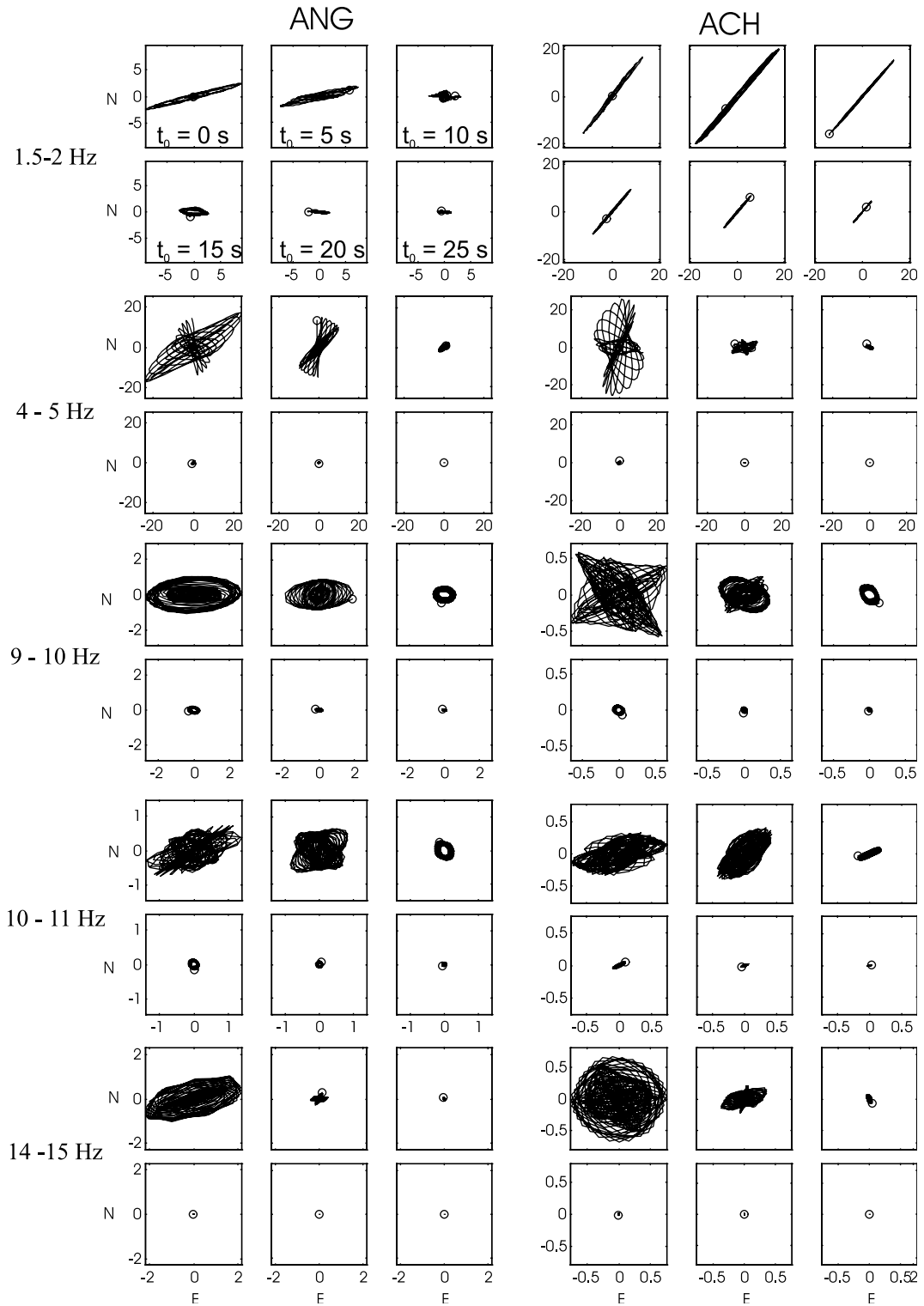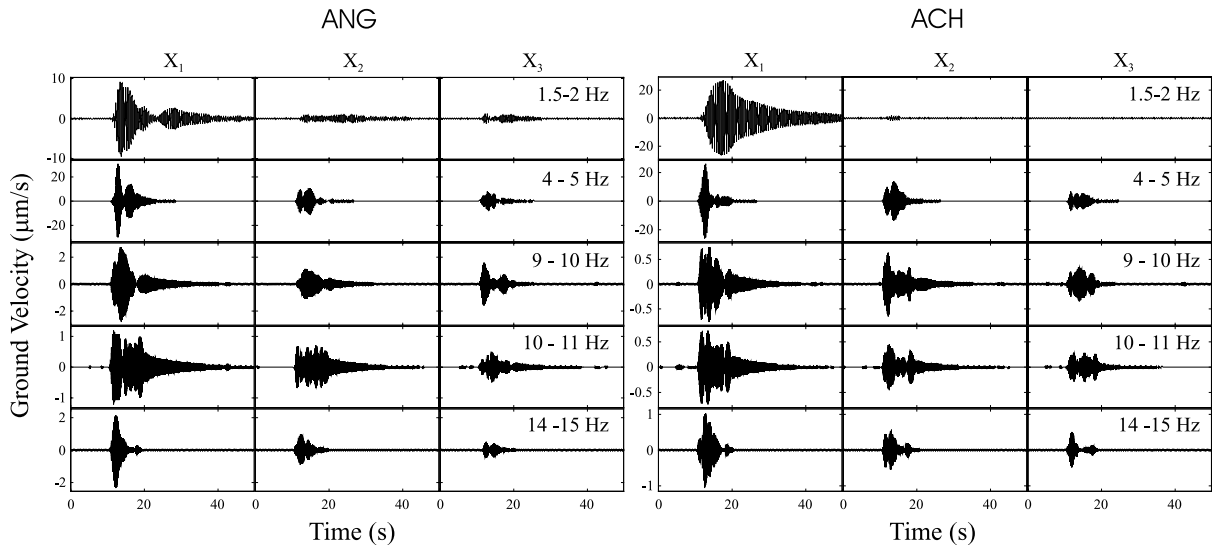
Fig. 10. Bandpass-filtered seismograms for the tornillo shown in Fig. 7, rotated to the optimum X_1–X_2–X_3 directions determined for each band. Filter limits are given in the figure. The left-hand display corresponds to the station ANG and the right-hand one to ACH. Ground velocity is given in μm/s.

example the lowest peak or those around 10 Hz. On the basis of this plot, we group the peaks found in this set of tornillos by their frequencies: 1.5–2, 2–5, 5–11, 11–15 and 15–20 Hz.

6. The polarization of multichromatic tornillos

In an effort to find the direction to the source of the tornillo on 8 January 2000, we plot the particle motion in the horizontal plane observed at the stations ANG and ACH for each peak (Fig. 9). The frequency bands given on the left-hand side of the figure indicate the filter limits used for each peak. Each diagram spans 5 s, so that the figure shows the polarization in each band for a total of 30 s. We observe that the polarization of the tornillo depends on the frequency band. For the peak between 1.5 and 2 Hz, which often has the largest amplitude, the polarization is nearly linear and remains almost

constant throughout the entire interval shown. While the polarization at ANG trends ENE–WSW, close to the direction to the active crater from this station, the particle motion at ACH points NE–SW. If we assume the ground motion is produced by P, S_V or Rayleigh-type waves, we can use the particle motion as an indication of the direction to the source. The polarizations measured at the two stations imply a source well to the WSW of the active crater. The assumption that the tornillo consists of S_H or Love waves does not suggest a more likely location for the source.

For the higher frequencies (Fig. 9), the polarization is neither necessarily linear nor constant. It is clear that the direction of polarization as well as the rectilinearity change at both stations as a function of time. Following Seidl and Hellweg (1991) and Hellweg (2000a,b), we analyze the suite of tornillos recorded at both stations in each to determine the azimuth, inclination and

Fig. 9. Bandpass-filtered particle motion diagrams in the *N–E* plane for the stations ANG (left) and ACH (right) for the five spectral peaks of the tornillo shown in Fig. 7. The limits of the filter for each peak are given by the labels on the left. For each station and frequency a set of six diagrams of 5 s each gives the particle motion for 30 s. In the top left set, the starting times given apply to each set. Amplitude is given in μm/s and is common for each set as shown on the axes.

rectilinearity of the particle motion for each peak, applying the covariance matrix method described by Matsumura (1981) and Kanasewich (1981). The values determined for the 15 tornillos for both stations are given in Table 1. For Fig. 10, the tornillo is bandpass-filtered to extract energy from one of the spectral peaks. In all cases, the passband of the filter, 0.5 Hz for the peak between 1.5 and 2 Hz, and 1 Hz for all peaks at higher frequencies, is much broader than the spectral width of the peak. This means that the effect on the phase of the narrow-band signals is minimal. The covariance matrix is determined from a data interval extending from the maximum in the band until the signal-to-noise ratio is low. The X_1–X_2–X_3 coordinate system is determined by the directions of the eigenvectors of the covariance matrix, with X_1 and X_3 corresponding to the largest and smallest eigenvectors and to the major and minor axes of the polarization ellipsoid, respectively. The Z–N–E components are then transformed to the X_1–X_2–X_3 coordinate system. Note that in the 1.5–2.0 Hz band at ACH, the separation of energy is quite successful, with very little amplitude remaining on the X_2 and X_3 components. On the other hand, at ANG, the coda is well-separated, while it is impossible to

rotate all the energy during the first 10 s to a single component. As can be expected from the elliptical particle motion for the high frequencies in Fig. 9, it is also impossible to segregate the energy of the tornillo in the 9–10 and 10.5–11.5 Hz bands completely to a single component in the rotated coordinate system.

In polarization analysis in seismology, the product of the radial and vertical components, RZ, is a diagnostic for wave-type (Plešinger et al., 1986). This product is positive for P waves, negative for S_V waves and for Rayleigh waves of frequency f, it oscillates with $2f$. Here, R is taken to be the horizontal component with the highest amplitude. Since the inclination for most spectral peaks is greater than 75°, they are nearly horizontal and R is approximately the X_1 component shown in Fig. 10. Fig. 11 shows the product RZ for the tornillo of 8 January 2000. Here, the tornillo, filtered to extract the signals in each of the five frequency bands, is rotated in the horizontal plane to achieve a maximum separation of energy. In all frequency bands, the RZ product oscillates with $2f$, indicating Rayleigh wave-like behavior. In fact, it does not matter whether we choose the rotated horizontal seismogram with the maximum amplitude to be R, or that with smallest
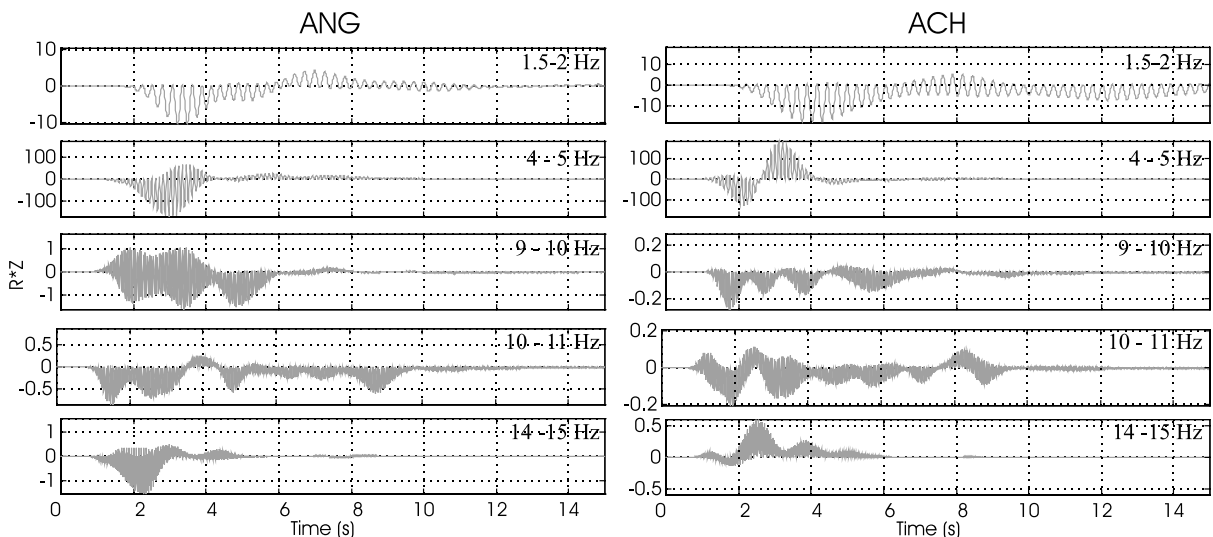

Fig. 11. RZ product for the tornillo shown in Fig. 7. R is taken to be the direction of the average polarization ellipse in the horizontal plane. Filter limits are given in the figure. The left-hand display corresponds to the station ANG and the right-hand one to ACH.

amplitude. The product of either with the Z seismogram oscillates with $2f$. This behavior is due to the ellipticity of the particle motion, and is an indication that the energy on any one component is out of phase with that on the other components. This is also the reason that no transformation can be found which rotates all the energy of the tornillo for a single peak onto a single component.

For these 15 tornillos we have determined the azimuth, inclination and rectilinearity for each peak using the method of Matsumura (1981). We compare the values determined at each station in Fig. 12. For the peaks between 1.5 and 2.0 Hz, the particle motion does not change very much from one tornillo to the next. This can be deduced from the very tight cluster of the azimuths measured at ANG as compared with ACH (Fig. 12a, diamonds). In addition, the inclination is nearly horizontal for all tornillos at both stations (Fig. 12b, diamonds), and nearly linearly polarized (Fig. 12c, diamonds). Particle motion for peaks in the band between 2.0 and 5.0 Hz cluster into two groups, one with an azimuth very similar to the 1.5–2.0 Hz peaks and a second group with an azimuth around 210° at ANG and around 30° at ACH (Fig. 12a, squares). The inclination for all the peaks in this band is nearly horizontal, but not nearly as clustered as for the lowest band (Fig. 12b, squares), while the rectilinearity is scattered, indicating much more elliptical motion with no particular relationship between that at ANG and ACH. For the higher bands, the particle motion cannot be described as being particularly constant from one tornillo to the next. The azimuths, inclinations and rectilinearity are scattered throughout the correlation plots. Perhaps the only generalization that can be made, is that even at
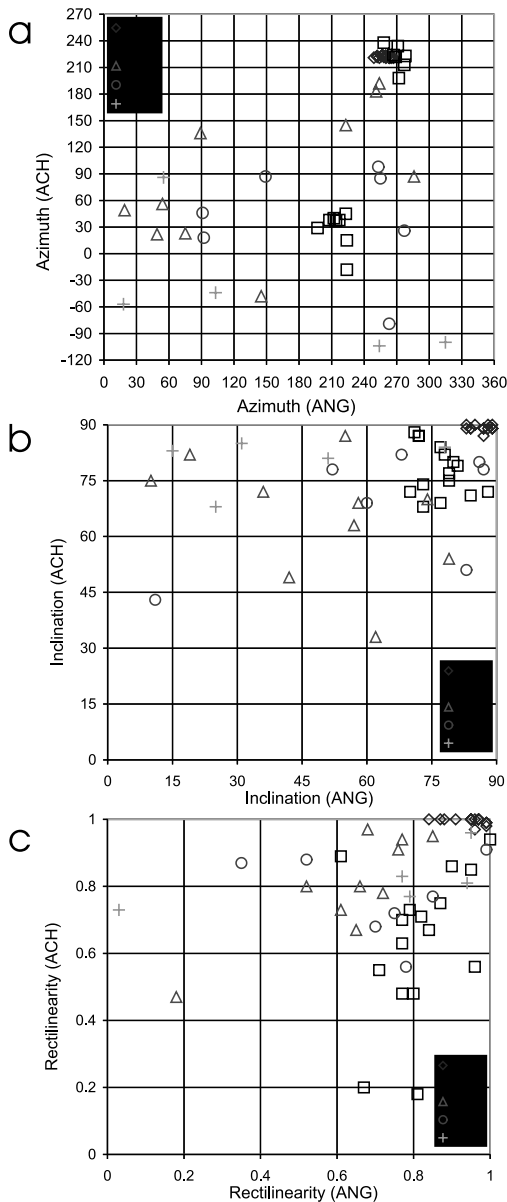
Fig. 12. (a) Comparison of the azimuth of the main axis of the polarization ellipsoid determined at ANG and ACH for the spectral lines present in all the tornillos from 5 January 2000 until 12 February 2000. Different spectral bands are represented by different symbols (diamonds = 1.5–2 Hz, squares = 2–5 Hz, triangles = 5–11 Hz, circles = 11–15 Hz and crosses = 15–20 Hz). Note the tight cluster for the 1.5–2 Hz band and the two tight clusters for the 2–5 Hz band. (b) Comparison of the inclination of the main axis of the polarization ellipsoid determined at ANG and ACH for the spectral lines present in all the tornillos from 5 January 2000 until 12 February 2000. Spectral band symbols as in panel a. Note the tight cluster for the 1.5–2 Hz band and that the 2–5 Hz band is more clustered than the higher frequencies. (c) Comparison of the rectilinearity of the polarization ellipsoid determined at ANG and ACH for the spectral lines present in all the tornillos from 5 January 2000 until 12 February 2000. Spectral band symbols as in panel a. Note the tight cluster for the 1.5–2 Hz band.
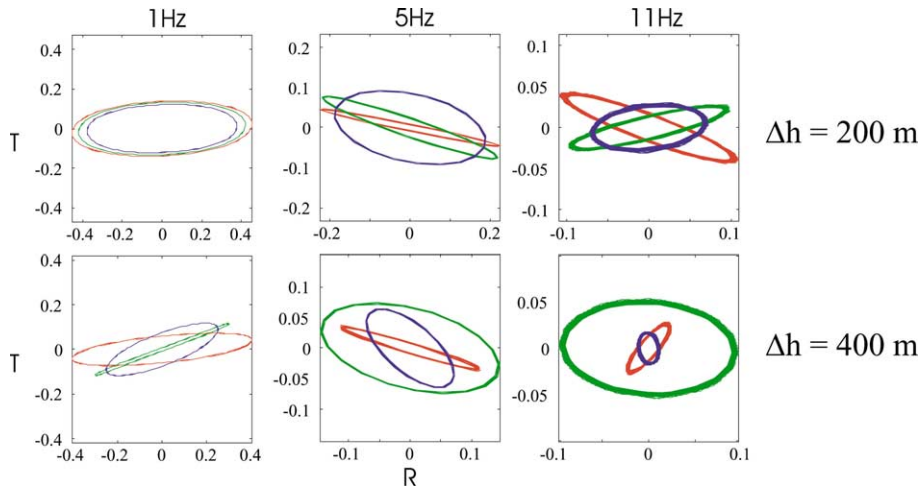
Fig. 13. Particle motion in the *R–T* plane for 1-, 5- and 11-Hz waves assuming acoustic scattering with 12 scatterers/km^3. In the top three plots, the source depth changes by 200 m between the red and green, and the green and blue ellipses, respectively. In the bottom plots, the depth step is 400 m.

the higher frequencies, the inclination at ACH tends to be more closely horizontal than at ANG.

What then, are the characteristics of the polarization of tornillos? For the peaks between 1.5 and 2 Hz, all tornillos have one prefered polarization direction at each station. These polarizations cannot be explained, however, as P, S or surface waves passing through a simple medium from a single point source located near the active crater, as they are neither radial nor transverse to that direction. At all frequencies, the waves share the characteristics of Rayleigh waves, in that the *RZ* product oscillates with 2*f*. While the overall particle motion for the peaks at frequencies below 5 Hz remains nearly the same from one tornillo to the next, it differs at higher frequencies. In addition, the polarization may change during the beginning of any given event at frequencies above 2 Hz.

The acoustic model for the effects of scattering on the polarization and amplitude of waves in the volcanic medium explains many of the characteristics we observe at the various frequencies present in the tornillos. Small changes in the overall configuration of the system consisting of source, scatterers and receiver will produce small differences in the polarization at low frequencies and larger differences as the frequency increases.

These changes in the particle motion encompass changes in the direction of the major axis of the polarization ellipsoid (azimuth and inclination) as well as the rectilinearity. If the particle motion is elliptical rather than linear, the product of either of the horizontal components with the *Z* component will oscillate with 2*f*, explaining the apparent similarity to Rayleigh waves.

While the particle motion remains relatively constant at low frequencies, at high frequencies, the particle motion changes during the course of an individual tornillo. It is not likely that the locations of the scatterers in the volcanic edifice would change appreciably during a single tornillo. However, if the source of the seismic waves moves, the polarization observed at the receiver will change as a function of time. Fig. 13 shows representatively how polarization can change if the scattering medium remains the same and the depth of the source changes. For these two realizations, I chose a model scattering medium with an acoustic velocity of 1000 m/s and 12 scatterers/km^3. The red, green and blue ellipses show the particle motion for three different source depths: 0, 200 and 400 m; or 0, 400 and 800 m, respectively. For these calculations the source–receiver distance is 1000 m. When the step is only 200 m, the change in polarization and amplitude for 1 Hz

waves is small. At 5 Hz, the rectilinearity changes appreciably, while the net amplitude, the direction of the particle motion and the rectilinearity all change for the 11 Hz waves. As may be expected, the effects are stronger when the change in depth is larger. Thus, if the medium parameters we have used for the model calculations are correct, the location of the source of the tornillo is constant to within about 200 m during a single tornillo. All tornillos are generated in a volume of the volcanic edifice less than 200 m in diameter.

7. Discussion

The acoustic model of single scattering with no attenuation demonstrates that even a simple system of scatterers can mimic important characteristics of the polarization observed for volcanic tremor and events. The coda present in shocks at Lascar Volcano (Asch et al., 1996; Hellweg, 1999a) and in volcano-tectonic events at Galeras Volcano (Seidl et al., 2003) indicate that scattering is an important process affecting the wavefields in these volcanoes. However, the scattering model only allows qualitative conclusions about the volcanic medium, due to the lack of information about such important parameters as the velocity structure. A comparison of the synthetics with the data from Lascar and Galeras leads to the conclusion that the medium must have many scatterers. These may be related to layers or other internal structures in the volcano or its topography. The effect of a small change in the location of the source depends very much on the wavelength we are observing. For low frequencies, and therefore relatively large wavelengths, there will be little change in the polarization, as the change in the wave-number phase is small. On the other hand, at high frequencies and concomitantly shorter wavelengths, a small change in the location of the source of the seismic waves will produce a large change in the polarization.

Unlike its application in earthquake seismology, polarization analysis of volcanic seismic signals cannot necessarily be used to determine wave type and the direction to the source. This is clear from the example of multichromatic tremor at Lascar Volcano. In this case, no one wave type could explain the particle motion observed for the various spectral peaks at the four stations near the volcano.

On the other hand, the example of the multichromatic tornillos recorded on Galeras Volcano shows that the polarization does contain important information about the source. For example, the polarization of the low-frequency peak, 1.5–2.0 Hz, changes very little during the course of the 15 tornillos. This implies that the tornillos from this episode are all generated at the same place in the volcano, probably always by the same process. The small changes in the particle motion at high frequencies during a single tornillo (Fig. 9) and from one tornillo to the next (Fig. 12), suggest that there are small changes in the position of the source, both during a single tornillo and from one tornillo to the next. If we assume a propagation velocity for the seismic waves in the volcano, we can estimate the maximum size of these location changes, since the polarization of waves with frequencies below 5 Hz changes very little. At a medium velocity of 1000 m/s this frequency corresponds to a wavelength of 200 m. The change in the source's location must be smaller than this.

References

Aki, K., Chouet, B., 1975. Origin of coda waves: source, attenuation, and scattering effects. J. Geophys. Res. 80, 3322–3342.

Asch, G., Bock, G., Gräber, F., Haberland, C., Hellweg, M., Kind, R., Rudloff, A., Wyllagalla, K., 1995. Passive Seismologie im Rahmen von PISCO'94, Sonderforschungsbereich 267 Deformationsprozesse in den Anden. Berichtband für die Jahre 1993-1995, Berlin, pp. 619–677.

Asch, G., Wylegalla, K., Hellweg, M., Seidl, D., Rademacher, H., 1996. Observations of rapid-fire event tremor at Lascar Volcano, Chile. Ann. Geofis. 39, 273–282.

Benoit, J., McNutt, S.R., 1997. New constraints on source processes of volcanic tremor at Arenal volcano, Costa Rica, using broadband seismic data. Geophys. Res. Let. 24, 449–452.

Gardeweg, M., Medina, E., 1994. La erupcion subpliniana del 19-20 de Abril de 1993 del Volcan Lascar, N. de Chile. Actas del 7. Congreso Geologico Chileno 1994, vol. 1, pp. 299–304.

Gil-Cruz, F., 1999. Observations of two special kinds of tremor at Galeras volcano, Colombia (1989-1991). Ann. Geofis. 42, 437–450.

Gómez, D.M., Torres, R.A., 1997. Unusual low-frequency volcanic seismic events with slowly decaying coda waves observed at Galeras and other volcanoes. J. Volcanol. Geotherm. Res. 77, 173–193.

Hagerty, M.T., Schwartz, S.Y., Protti, J., Garces, M., Dixon, T., 1997. Observations at Costa Rican volcano offer clues to causes of eruptions. EOS Trans. AGU 78, 570.

Hellweg, M., 1999a. Seismic signals from Lascar Volcano. J. S. Am. Earth Sci. 12, 123–133.

Hellweg, M., 1999b. Listening carefully: Unique observations of harmonic tremor at Lascar volcano, Chile. Ann. Geofis. 42, 451–464.

Hellweg, M., 2000a. Volcanic tremor and physical source models: Lascar Volcano, Chile. Doctoral Thesis. Berichte des Instituts für Geophysik der Universität Stuttgart 14, 132 pp.

Hellweg, M., 2000b. Physical models for the source of Lascar's harmonic tremor. J. Volcanol. Geotherm. Res. 101, 183–198.

Ingard, K.U., 1988. Fundamentals of Waves and Oscillations. Cambridge University Press, Cambridge, 595 pp.

Kanasewich, E.R., 1981. Time Sequence Analysis in Geophysics. The University of Alberta Press, Alberta.

Lees, J.J., Johnson, J., Gordeev, E., Batereau, K., Ozerov, A., 1997. Volcanic explosions at Karymsky: A Broadband experiment around the cone. EOS Trans. AGU 78, Fall Meeting Suppl., F430.

Matsumura, S., 1981. Three-dimensional expression of seismic particle motions by the trajectory ellipsoid and its application to the seismic data observed in the Kanto district, Japan. J. Phys. Earth 29, 221–239.

Narváez, M.L., Torres, R.A., Gómez, D.M., Cortés, G.P.J., Cepeda, H.V., Stix, J., 1997. Tornillo-type seismic signals at Galeras volcano, Colombia, 1992-1993. J. Volcanol. Geotherm. Res. 77, 159–171.

Neuberg, J., Pointer, T., 2000. Effects of volcano topography on seismic broad-band waveforms. Geophys. J. Int. 143, 239–248.

Nuttli, O., 1961. The effect of the Earth's surface on the S wave particle motion. Bull. Seismol. Soc. Am. 51, 237–246.

Nuttli, O., Whitmore, J.D., 1961. An observational determination of the variation of the angle of incidence of P waves with epicentral distance. Bull. Seismol. Soc. Am. 51, 269–276.

Ortega, A.M., 2000. Descripcion de los Episodios Eruptivos y de Emision Correspondientes a la Actividad del Vulcan Galeras durante el Ano 2000. INGEOMINAS Report, 14 pp.

Plešinger, A., Hellweg, M., Seidl, D., 1986. Interactive high-resolution polarization analysis of broad-band seismograms. J. Geophys. 59, 129–139.

Schlindwein, V., Wassermann, J., Scherbaum, F., 1995. Spectral analysis of harmonic tremor signals at Mt. Semeru volcano, Indonesia, 1995. Geophys. Res. Lett. 22, 1685–1688.

Seidl, D., Hellweg, M., 1991. Volcanic tremor recordings: polarization analysis. In: Schick, R., Mugiono, R. (Eds.), Volcanic Tremor and Magma Flow. Forschungszentrum Jülich GmbH, pp. 31–46.

Seidl, D., Hellweg, M., Calvache, M., Gómez, D., Ortega, A., Torres, R., Böker, F., Buttkus, B., Faber, E., Greinwald, S., 2003. The multiparameter station at Galeras Volcano (Colombia): concept and realization. J. Volcanol. Geotherm. Res. 125, 1–12.

Torres, R.A., Gómez, D.M., Narváez, M.L., 1996. Unusual seismic signals associated with the activity at Galeras volcano, Colombia, from July 1992 to September 1994. Ann. Geofis. 39, 299–310.